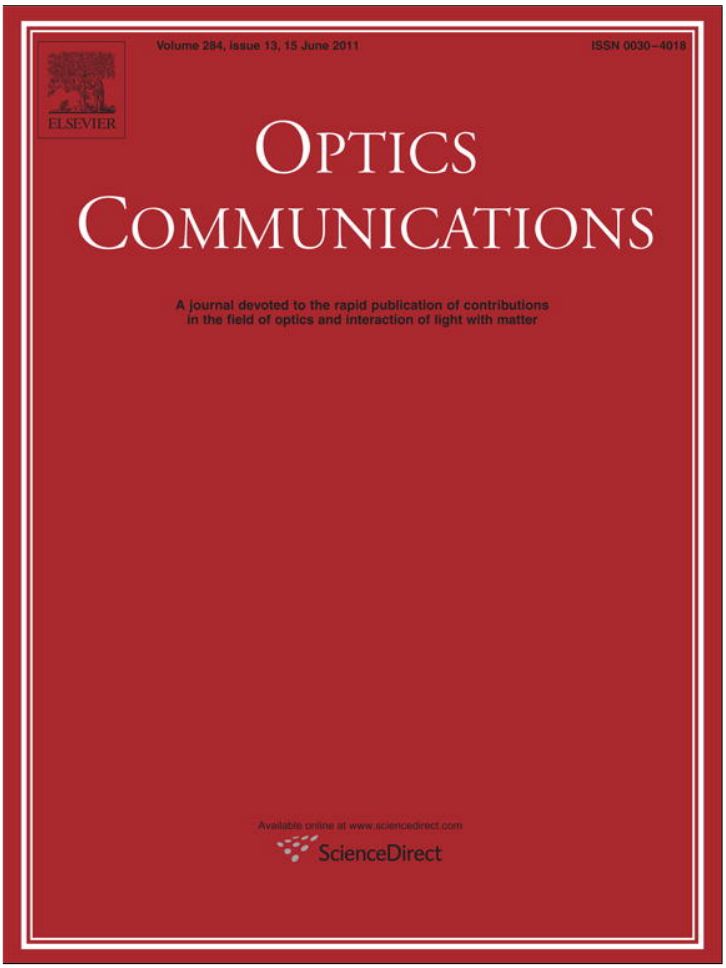

Optics Communications 284 (2011) 3408–3415

Contents lists available at ScienceDirect

Optics Communications

journal homepage: www.elsevier.com/locate/optcom

Evolution of first-order sidebands from multiple FWM processes in HiBi optical fibers

Nuno A. Silva [a,b,*], Nelson J. Muga [a,c], Armando N. Pinto [a,b]

[a] Instituto de Telecomunicações, Campus Universitário de Santiago, 3810-193 Aveiro, Portugal
[b] Departamento de Electrónica, Telecomunicações e Informática, Universidade de Aveiro, 3810-193 Aveiro, Portugal
[c] Departamento de Física, Universidade de Aveiro, 3810-193 Aveiro, Portugal

ARTICLE INFO

Article history:
Received 7 September 2010
Received in revised form 8 February 2011
Accepted 9 February 2011
Available online 5 March 2011

Keywords:
Nonlinear fiber optics
Multiple four-wave mixing
Stimulated Raman scattering

ABSTRACT

The generation of two idler waves inside a high birefringent (HiBi) optical fiber through three four-wave mixing (FWM) processes is studied theoretically. The coupled-equations for the field amplitudes are derived and analytically solved, in the co-polarized and orthogonal polarization schemes. The obtained solutions take into account the delayed Raman response of the medium. The polarization sensitivity of the generation of the idler waves is analyzed. Results show that the stimulated Raman scattering does not change the efficiency of the idler wave generation in the co-polarized scheme, whereas in the orthogonal polarization scheme that nonlinear process decreases the efficiency of the four-wave mixing processes. Results also show that this set of multiple four-wave mixing processes is physically quite different from the typical single or dual pump four-wave mixing configurations. Findings show that the power transfer from the pumps to the idler fields can lead to a monotonous growth, or a periodic evolution of the sidebands along the fiber. Results show that the process efficiency varies greatly with the angle between the two pump polarizations.

1. Introduction

The nonlinear response of optical fibers can be described by a complex third-order nonlinear response function, $R^{(3)}_{ijkl}$ [1]. The real part of $R^{(3)}_{ijkl}$ is related to the nonresonant electronic response, and gives rise to nonlinear processes such as stimulated four-wave mixing (FWM), whereas the imaginary part is related to resonant (nuclear) response, and leads to the process of Raman amplification [1–3]. Stimulated Raman scattering (SRS) in optical fibers is a nonlinear process in which the optical frequencies from incident pumps are converted to lower frequencies (Stokes amplification), and higher frequencies (anti-Stokes amplification) through molecular vibrations [1,4]. Stimulated FWM is a nonlinear process in which photons from two or more frequencies launched into the fiber are annihilated, and new photons are created at new or at already existing frequencies in the fiber [1]. Efficient stimulated FWM demands phase-matching. In order to achieve that condition, most of the work related with FWM has been done around the fiber zero-dispersion wavelength [5–7].

The unique properties of photonic crystal fibers (PCFs) have opened a new range of applications of nonlinear effects for all-optical signal processing [8]. Indeed, applications such as optical parametric amplification [9], wavelength conversion [10], signal regeneration [11], supercontinuum generation [12] and optical demultiplexing [13] can be obtained very efficiently in this kind of fibers. PCFs can combine a high nonlinear coefficient with a polarization maintaining structure, characterized by a modal birefringence of the order of $\delta n \sim 10^{-4}$ [13,14]. Therefore, with PCFs it is possible to have a HiBi optical fiber with a strong nonlinear response of the medium [8]. Besides that, PCFs can also present a zero-dispersion wavelength in the infrared region of the spectrum, around 1550 nm [14]. The combination of these properties in a unique fiber provides the opportunity to obtain both stimulated FWM and SRS processes very efficiently [1,15]. Moreover, the high value of the nonlinear coefficient in PCFs allows nonlinear optical signal processing in short fiber lengths and in a low power regime [8]. An accurate description of these nonlinear processes in HiBi optical fibers can guide the development of new all-optical signal processing devices.

Typically, the single or dual pump FWM process involves only the generation of a new frequency. In these configurations, several studies of FWM process in optical fibers have been carried out, taken into account the quasi-instantaneous response of the nonlinear dielectric medium [16–18] and the delayed Raman response [19–22]. For fiber lengths on the order of the effective length of interaction, the optical fiber can be considered an almost lossless medium. In that limit several new frequencies are generated inside the fiber through multiple FWM processes [23]. The multiple FWM processes in optical fibers were investigated in Refs. [23–25], and their work was later extended to investigate the conservation law [26] and the nonlinear dynamics [27] of dual frequency-pumped multiple FWM processes, as well as to describe the dynamical evolution of the sidebands along an optical fiber [28]. Subsequent studies explored the interactions between pumps and the generated sidebands in highly birefringent fibers [29], and the role of stochasticity on multiple FWM processes [30]. Recently, the self-stability function of multiple FWM processes

* Corresponding author at: Instituto de Telecomunicações, Campus Universitário de Santiago, 3810–193 Aveiro, Portugal. Tel.: +351 234 377 900; fax: +351 234 377 901.
E-mail address: nasilva@av.it.pt (N.A. Silva).

0030-4018/$ – see front matter © 2011 Elsevier B.V. All rights reserved.
doi:10.1016/j.optcom.2011.02.014

was studied in Ref. [31], and their work has extended in order to describe this process in the presence of multifrequency pumps [32]. In Ref. [22], we studied the influence of the SRS on the generation of one idler wave through the stimulated FWM process in the single and dual pump configurations. Potential applications of these nonlinear processes are wavelength converters [33,34], modulation instability [29,35], demultiplexing [36,37] and phase conjugation [38,39].

Existing theories cannot fully describe the simultaneous generation of two idler waves through multiple FWM processes in optical fibers. For this reason, numerical solution of the nonlinear Schrödinger (NLS) equation is used for explain the experimental data [23–32]. In this paper we develop a theoretical model capable of describing the generation of two idler waves inside a birefringent optical fiber through three FWM processes, in both co-polarized and orthogonal polarization schemes. The obtained results take into account the delayed Raman response of the fiber. We use our model to quantify the impact of the delayed Raman response of the fiber on the generation of the two idler waves through three FWM processes. Since our theoretical model is vectorial, we are able to describe the evolution of the idler waves as a function of the polarization angle between the two pumps.

This paper contains five sections. Section 2 reviews the formalism of NLS equation and the third-order nonlinearities in optical fibers. In Section 3 we derive and solve analytically the combined processes of SRS and multiple FWM in two different polarization schemes. Section 4 describes the evolution of the first-order sidebands generated through multiple FWM processes as a function of the angle between the two pump polarizations. The main results presented in this paper are summarized in Section 5.

2. Analytical model

The evolution of the electrical field complex amplitudes, $A_i(z,t)$, inside an almost lossless birefringent optical fiber is governed by the NLS equation [22,40]

$$\frac{\partial A_i(z,t)}{\partial z} = \sum_{m=0}^{+\infty} \frac{i^{m+1}\beta_{m,i}}{m!}\frac{\partial^m A_i(z,t)}{\partial t^m} + i\gamma A_j(z,t)\int_{-\infty}^{+\infty} R^{(3)}_{ijkl}(\tau)A^*_k(z,t-\tau)A_l(z,t-\tau)d\tau, \tag{1}$$

where $\beta_{m,i}$ is the mth order dispersion coefficient for the x or y fiber axis, γ is the nonlinear parameter, and $R^{(3)}_{ijkl}$ is the fiber nonlinear response function [22,41,42]

$$R^{(3)}_{ijkl}(\tau) = \frac{1-f_R}{3}\delta(\tau)\left(\delta_{ij}\delta_{kl}+\delta_{ik}\delta_{jl}+\delta_{il}\delta_{jk}\right) + f_R R_a(\tau)\delta_{ij}\delta_{kl} + \frac{f_R}{2}R_b(\tau)\left(\delta_{ik}\delta_{jl}+\delta_{il}\delta_{jk}\right), \tag{2}$$

with

$$R_a(\tau) = f_a\frac{\tau_1^2+\tau_2^2}{\tau_1\tau_2^2}exp(-\tau/\tau_2)\sin(\tau/\tau_1)\Theta(\tau), \tag{3a}$$

$$R_b(\tau) = f_b\frac{1}{\tau_b}\left(2-\frac{\tau}{\tau_b}\right)\exp(-\tau/\tau_b)\Theta(\tau) + f_c\frac{\tau_1^2+\tau_2^2}{\tau_1\tau_2^2}\exp(-\tau/\tau_2)\sin(\tau/\tau_1)\Theta(\tau). \tag{3b}$$

In Eqs. (2), (3a) and (3b), $\Theta(\tau)$ is the Heaviside function, $f_R=0.245$ represents the fractional contribution of the delayed Raman response to the nonlinear refractive index, $\tau_1\simeq 12.2$ fS, $\tau_2\simeq 32.2$ fS, $\tau_b\simeq 96$ fS, $f_a=0.75$, $f_b=0.21$ and $f_c=0.04$ are typical values for silica based fibers [19,42].

In this work we are operating around the fiber zero-dispersion wavelength, and we are assuming a typical HiBi optical fiber with the following parameters: $\gamma=11\ W^{-1}km^{-1}$, zero-dispersion wavelength $\lambda_0=1550.5$ nm, $\delta n=10^{-5}$, third and fourth-order dispersion coefficients at zero-dispersion wavelength $\beta_{3,x}=\beta_{3,y}=-2.84\times10^{-2}$ ps^3/km and $\beta_{4,x}=\beta_{4,y}=2.99\times10^{-4}$ ps^4/km [13–15,43] and length $L=500$ m. We are also assuming a continuous input optical power per pump of $P_1=P_2=P_p=15$ mW.

3. Multiple four-wave mixing

Using the model presented in Section 2, we analyze in this section the generation of two new frequencies inside a HiBi optical fiber through the multiple FWM processes. In this study, two pumps (at ω_1 and ω_2) are launched into a fiber, giving rise to two new frequencies, ω_3 and ω_4, through three FWM processes, two degenerated and one non-degenerated. The two degenerated processes are given by $\omega_3=2\omega_1-\omega_2$ and $\omega_4=2\omega_2-\omega_1$, whereas the non-degenerated is given by $\omega_1+\omega_2=\omega_3+\omega_4$. These multiple FWM processes can be decomposed in two different polarization schemes, see Fig. 1.

We assume that the pumps are always much more intense than the idlers, and it is also assumed that the fiber length is much shorter than the walk-off length [1]. In that regime, we can apply the quasi-continuous wave approximation and the total optical field can be written as

$$A_j(z,t) = \sum_N A_{N,j}(z)\exp\{-i\Omega_N t\}, \tag{4}$$

where $N=1,2,3,4$ represents all fields in the j state of polarization, and $\Omega_N=\omega_N-\omega_0$, with ω_0 being the fiber zero-dispersion frequency of the fiber.

Substituting Eq. (4) in Eq. (1), the NLS equation for the pump fields, can be written as

$$\frac{\partial A_{u,j}(z)}{\partial z} = ik_j(\omega_u)A_{u,j}(z) + i\gamma P_{u,j}(z)A_{u,j}(z) + + i\gamma\xi_m\left(\Omega_{u,v}\right)P_{v,l}(z)A_{u,j}(z), \tag{5}$$

where $u,v=1,2$ represent the two pumps, according with the notation used in Fig. 1, with $u\neq v$, $\xi_m=\xi_\parallel$ for the co-polarized scheme, see Fig. 1a, and $\xi_m=\xi_\perp$ for the orthogonal polarization scheme, see Fig. 1b. In Eq. (5), $l=j=x$ for the co-polarized scheme. In the orthogonal polarization scheme $j=x$ and $l=y$ for $u=1$, whereas for $u=2$ we have $j=y$ and $l=x$. Finally, $P_{u,j}(z)=|A_{u,j}(z)|^2$ is the optical power of each pump field, and

$$k_j(\omega_u) = \sum_{m\geq 0}\frac{\beta_{m,j}}{m!}\Omega_u^m, \tag{6}$$

$$\xi_\parallel\left(\Omega_{u,v}\right) = 2-f_R+f_R\left(\tilde{R}_a\left(\Omega_{u,v}\right)+\tilde{R}_b\left(\Omega_{u,v}\right)\right), \tag{7}$$

$$\xi_\perp\left(\Omega_{u,v}\right) = 2\frac{1-f_R}{3}+f_R\tilde{R}_a(0)+\frac{f_R}{2}\tilde{R}_b\left(\Omega_{u,v}\right), \tag{8}$$

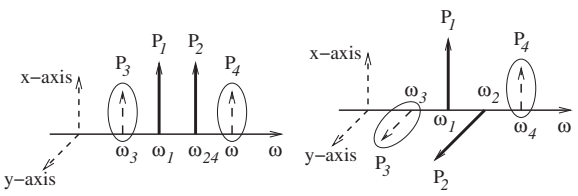

a) Co-polarized scheme. b) Orthogonal polarization scheme.

Fig. 1. Polarization schemes of the multiple FWM processes in the dual pump configuration.

where $\tilde{R}_a(\Omega)$ is the Fourier transform of $R_a(\tau)$, and $\tilde{R}_b(\Omega)$ is the Fourier transform of $R_b(\tau)$, and $\Omega_{u,v}=\omega_u-\omega_v$. After some mathematical manipulation, the complex amplitude for the pump fields at a distance z in the fiber can be written as

$$A_{u,j}(z) = A_{u,j}e^{i\left(k_j(\omega_u)-\gamma H_j(\omega_u)\right)z}F_j(0)^{-i\gamma G_j(\omega_u)} \times F_j(z)^{i\gamma G_j(\omega_u)}, \tag{9}$$

where $A_{u,j}$ is the input pump amplitudes, and

$$H_j(\omega_u) = \frac{P_{v,l}g_{Rm}^2\left(\Omega_{u,v}\right) + P_{u,j}g_{Rm}^2\left(\Omega_{v,u}\right)\xi_m\left(\Omega_{u,v}\right)}{g_{Rm}\left(\Omega_{u,v}\right)g_{Rm}\left(\Omega_{v,u}\right)}, \tag{10a}$$

$$G_j(\omega_u) = \frac{g_{Rm}\left(\Omega_{u,v}\right) + g_{Rm}\left(\Omega_{v,u}\right)\xi_m\left(\Omega_{u,v}\right)}{g_{Rm}\left(\Omega_{u,v}\right)g_{Rm}\left(\Omega_{v,u}\right)}, \tag{10b}$$

$$F_j(z) = g_{Rm}\left(\Omega_{2,1}\right)P_{1,x}e^{g_{Rm}\left(\Omega_{2,1}\right)P_{1,x}z} - g_{Rm}\left(\Omega_{1,2}\right)P_{2,l}e^{g_{Rm}\left(\Omega_{1,2}\right)P_{2,l}z}, \tag{10c}$$

where $g_{Rm}=g_{R||}$ for the co-polarized scheme, whereas for the orthogonal polarization scheme $g_{Rm}=g_{R\perp}$, and $P_{u,j}$ represents the input pump power.

From Eq. (9), we observe that the two pumps can transfer energy between them through the process of SRS. However, if the pumps are placed closely, $\Omega_{u,v}/2\pi<3$ THz, and if their power is maintained at a low level [22,44], the power transfer between the pumps is very small [22]. In that case, Eq. (9) can be written as

$$A_{u,j}(z) = A_{u,j}e^{i\left(k_j(\omega_u)+\gamma P_{u,j}+\gamma\xi_m(0)P_{v,l}\right)z}. \tag{11}$$

3.1. Idlers evolution in the co-polarized scheme

The evolution of the idler fields in the co-polarized scheme is governed by the NLS equation, obtained from Eqs.(1) and (4)

$$\frac{\partial A_{\alpha,x}(z)}{\partial z} = i\left[k_x(\omega_\alpha)+\gamma\xi_\parallel\left(\Omega_{\alpha,1}\right)P_{1,x}\right]A_{\alpha,x}(z) + i\gamma\xi_\parallel\left(\Omega_{\alpha,2}\right)P_{2,x}A_{\alpha,x}(z) + i\gamma\rho_\parallel\left(\Omega_{\alpha,u}\right)A_{u,x}^2(z)A_{v,x}^*(z) + i\gamma\eta_\parallel(\omega_\alpha)A_{1,x}(z)A_{2,x}(z)A_{\sigma,x}^*(z), \tag{12}$$

where $\alpha\neq\sigma=3,4$ represent the two idlers, according with the notation used in Fig. 1, $u\neq v=1,2$, with $u=1$ for $\alpha=3$ and $u=2$ for $\alpha=4$, and

$$\rho_\parallel\left(\Omega_{\alpha,u}\right) = 1-f_R+f_R\left(\tilde{R}_a\left(\Omega_{\alpha,u}\right)+\tilde{R}_b\left(\Omega_{\alpha,u}\right)\right), \tag{13}$$

$$\eta_\parallel(\omega_\alpha) = 2(1-f_R)+f_R\left(\tilde{R}_a\left(\Omega_{\alpha,u}\right)+\tilde{R}_b\left(\Omega_{\alpha,u}\right)\right) + f_R\left(\tilde{R}_a\left(\Omega_{\alpha,v}\right)+\tilde{R}_b\left(\Omega_{\alpha,v}\right)\right). \tag{14}$$

The evolution of the complex amplitudes of both idlers at a distance z in the fiber is given by

$$P_{\alpha,x}(z) = |A_{\alpha,x}(z)|^2 = \left|\left\{e^{i\mathbb{k}_x(\omega_\alpha)z}\left[i\frac{\gamma\rho_\parallel\left(\Omega_{\alpha,u}\right)}{g_x(\omega_\alpha)}A_{u,x}^2A_{v,x}^* \times\sinh\left(g_x(\omega_\alpha)z\right)+\Theta_{\alpha,x}\left(i\frac{\mathbb{k}_x(\omega_\alpha)}{g_x(\omega_\alpha)}\sinh\left(g_x(\omega_\alpha)z\right) -\cosh\left(g_x(\omega_\alpha)z\right)\right)\right]+\Theta_{\alpha,x}\right\}\Phi_{\alpha,x}(z)\right|^2, \tag{15}$$

where both idlers were assumed to have no optical power at $z=0$, and

$$\Phi_{\alpha,x}(z) = e^{i\left(2k_x(\omega_u)-k_x(\omega_v)\ +\ 3\gamma P_{v,x}\right)z}, \tag{16a}$$

$$\mathbb{k}_x(\omega_3) = \left[\Delta\beta_{x1}-\Delta\beta_{x2}+\gamma\left(P_{1,x}-P_{2,x}\right) \times\left(\xi_\parallel\left(\Omega_{3,1}\right)-\xi_\parallel\left(\Omega_{3,2}\right)+3\right)\right]/2, \tag{16b}$$

$$\mathbb{k}_x(\omega_4) = \left[\Delta\beta_{x2}-\Delta\beta_{x1}+\gamma\left(P_{2,x}-P_{1,x}\right) \times\left(\xi_\parallel\left(\Omega_{4,2}\right)-\xi_\parallel\left(\Omega_{4,1}\right)+3\right)\right]/2, \tag{16c}$$

$$g_x^2(\omega_\alpha) = \left(\gamma\eta_\parallel(\omega_\alpha)\right)^2P_{1,x}P_{2,x}-\frac{1}{4}\left[\Delta\beta_{x3} +\gamma\left(P_{1,x}+P_{2,x}\right)\left(\xi_\parallel\left(\Omega_{\alpha,u}\right)+\xi_\parallel\left(\Omega_{\alpha,v}\right)-3\right)\right]^2. \tag{16d}$$

In Eq. (15), $\Theta_{3,x}$ and $\Theta_{4,x}$ are given by

$$\Theta_{3,x} = \frac{\gamma^2\eta_\parallel(\omega_3)\rho_\parallel\left(\Omega_{3,1}\right)P_{2,x}A_{1,x}^2A_{2,x}^*}{\delta_\parallel(\omega_3)\varphi_\parallel(\omega_3)-\left(\gamma\eta_\parallel(\omega_3)\right)^2P_{1,x}P_{2,x}} -\frac{\gamma\varphi_\parallel(\omega_3)\rho_\parallel\left(\Omega_{3,1}\right)A_{1,x}^2A_{2,x}^*}{\delta_\parallel(\omega_3)\varphi_\parallel(\omega_3)-\left(\gamma\eta_\parallel(\omega_3)\right)^2P_{1,x}P_{2,x}}, \tag{17a}$$

$$\Theta_{4,x} = \frac{\gamma^2\eta_\parallel(\omega_4)\rho_\parallel\left(\Omega_{4,2}\right)P_{1,x}A_{2,x}^2A_{1,x}^*}{\delta_\parallel(\omega_4)\varphi_\parallel(\omega_4)-\left(\gamma\eta_\parallel(\omega_4)\right)^2P_{1,x}P_{2,x}} -\frac{\gamma\delta_\parallel(\omega_4)\rho_\parallel\left(\Omega_{4,2}\right)A_{2,x}^2A_{1,x}^*}{\delta_\parallel(\omega_4)\varphi_\parallel(\omega_4)-\left(\gamma\eta_\parallel(\omega_4)\right)^2P_{1,x}P_{2,x}}, \tag{17b}$$

where

$$\delta_\parallel(\omega_\alpha) = \Delta\beta_{x1}+\gamma\xi_\parallel\left(\Omega_{\alpha,u}\right)P_{1,x}+\gamma P_{2,x}\left(\xi_\parallel\left(\Omega_{\alpha,v}\right)-3\right), \tag{18a}$$

$$\varphi_\parallel(\omega_\alpha) = \Delta\beta_{x2}+\gamma\xi_\parallel\left(\Omega_{\alpha,u}\right)P_{2,x}+\gamma P_{1,x}\left(\xi_\parallel\left(\Omega_{\alpha,v}\right)-3\right). \tag{18b}$$

From Eqs. (15) to (18a and 18b) we can see that the efficiency of the three FWM processes are governed by three phase-matching conditions [1,43]

$$\Delta\beta_{x1} = k_x(\omega_3)+k_x(\omega_2)-2k_x(\omega_1) = (\omega_1-\omega_0)(\omega_1-\omega_2)^2\beta_{3,x} +\frac{1}{2}(\omega_1-\omega_2)^2\left[(\omega_1-\omega_0)^2+\frac{1}{6}(\omega_1-\omega_2)^2\right]\beta_{4,x}, \tag{19a}$$

$$\begin{aligned}\Delta\beta_{x2} &= k_x(\omega_4) + k_x(\omega_1) - 2k_x(\omega_2)\\ &= (\omega_2-\omega_0)(\omega_2-\omega_1)^2\beta_{3,x}\\ &\quad + \frac{1}{2}(\omega_2-\omega_1)^2\left[(\omega_2-\omega_0)^2 + \frac{1}{6}(\omega_2-\omega_1)^2\right]\beta_{4,x},\end{aligned} \tag{19b}$$

$$\Delta\beta_{x3} = \Delta\beta_{x1} + \Delta\beta_{x2}. \tag{19c}$$

In Fig. 2, we plot the optical power evolution of both idler waves, given by Eq. (15), as a function of wavelength separation between the two pump fields, $\lambda_1-\lambda_2$. In Fig. 2a and b, we plot the evolution of the idler field at frequency ω_3, whereas in Fig. 2c and d, we present the evolution of the idler at frequency ω_4, see the scheme of Fig. 1a. In Fig. 2, we can see that the influence of the delayed Raman response on the idler waves is negligible in these cases. This shows that the process can mainly be described by the FWM phase-matching conditions, given by Eqs. (19a), (19b) and (19c). In the situations considered in Fig. 2, at least one of the phase-matching conditions is not null. According to Ref. [22], if the nonlinear process remains unmatched, the limit $f_R=0$ is a good approximation to describe it, which is the case.

In Fig. 2a and c, we plot the evolution of the optical power $P_{3,x}(L)$ and $P_{4,x}(L)$, respectively, for two cases: $\lambda_1=\lambda_0$, and $\lambda_2=\lambda_0$. For $\lambda_1=\lambda_0$ we have $\Delta\beta_{x1}\approx 0$, and for $\lambda_2=\lambda_0$ we have $\Delta\beta_{x2}\approx 0$. In both cases, there exist two FWM processes that remain unmatched. We observe from Fig. 2(a) and (c) that the phase-matching condition $\Delta\beta_{x1}\approx 0$ (with $\Delta\beta_{x2}\neq 0$) leads to a high efficient generation of the ω_3 idler wave, and to a less efficient generation of the ω_4 idler wave. The opposite happens when $\Delta\beta_{x2}\approx 0$ (with $\Delta\beta_{x1}\neq 0$). This is due to the major or minor separation between the idler wave and the pump in the fiber zero-dispersion. It can be seen in Fig. 2(a) that, for $\lambda_1=\lambda_0$ the optical power of the idler wave ω_3 increases with the wavelength separation until $\lambda_1-\lambda_2\approx 7.5$ nm. However, in Fig. 2(c) we can observe that for $\lambda_2=\lambda_0$ the optical power of idler wave decreases with the wavelength separation between the pumps, and reaches a local minimum when $\lambda_1-\lambda_2\approx 7.5$ nm. This arises from the $\Theta_{\alpha,x}$ contribution present in Eq. (15), that gives rise to the multiple FWM processes. This happens because the phase-matching conditions for the idler wave in Fig. 2(a) remains approximately zero for the wavelength range considered, which leads to a high value of $\Theta_{3,x}$. The optical power increases due to the fact that the generation of the idler wave in the anomalous-dispersion regime is more efficient than in the normal-dispersion regime. In Fig. 2(c), the phase-matching conditions are also satisfied. However, we are in the normal-dispersion regime, and in that case the generation of the idler is inefficient, when compared with the anomalous-regime. These results show that the optical power of the idler wave can increase with the wavelength separation, because in the multiple FWM processes, Fig. 2(a), we are not only transferring energy from the pump $P_{1,x}$ for $P_{3,x}$ but also from the pump $P_{2,x}$, and the two pumps also transfer energy between them (Eq. (11)). This means that until $\Delta\beta_{x2}$ and $\Delta\beta_{x3}$ starts to deviate significantly from zero, the multiple FWM processes continue to amplify the idler wave, Fig. 2(a). The results presented in Fig. 2(a) for $\lambda_2=\lambda_0$, and in Fig. 2(c) for $\lambda_1=\lambda_0$, also show that, the optical power of the idler wave rapidly decreases with the increase of $\lambda_1-\lambda_2$. This is due to the fact that the phase-matching conditions start to deviates from zero.

In Fig. 2(b) and (d), we plot the evolution of the optical power $P_{3,x}(L)$ and $P_{4,x}(L)$, respectively, for two cases: $\lambda_1=1552$ nm and $\lambda_2=1552$ nm. We can see from Fig. 2(b) and (d) that the case of $\lambda_1=1552$ nm leads to a high efficient generation of the idler wave ω_3, and a less efficiency in the generation of ω_4. The opposite happens for $\lambda_2=1552$ nm. It can also be seen in Fig. 2(b) that for $\lambda_2=1552$ nm the optical power of the idler wave decreases more rapidly with the evolution of $\lambda_1-\lambda_2$, than for $\lambda_1=1552$ nm. The opposite result occurs when we analyze the idler wave ω_4, see Fig. 2(d). This happens because the difference $\lambda_1-\lambda_0$ is smaller for $\lambda_1=1552$ nm than for $\lambda_2=1552$ nm, in Fig. 2(b), and the opposite happens in Fig. 2(d).

In Fig. 3, we plot the optical power evolution of both idler waves, given by Eq. (15), along the fiber length, for the case $\lambda_1=\lambda_0$ and $\lambda_2=1542.5$ nm. It can be seen in Fig. 3 that the optical power of the idler wave at frequency ω_3, $P_{3,x}(z)$, grows monotonically along the length of the fiber, which is in line with numerical results presented in

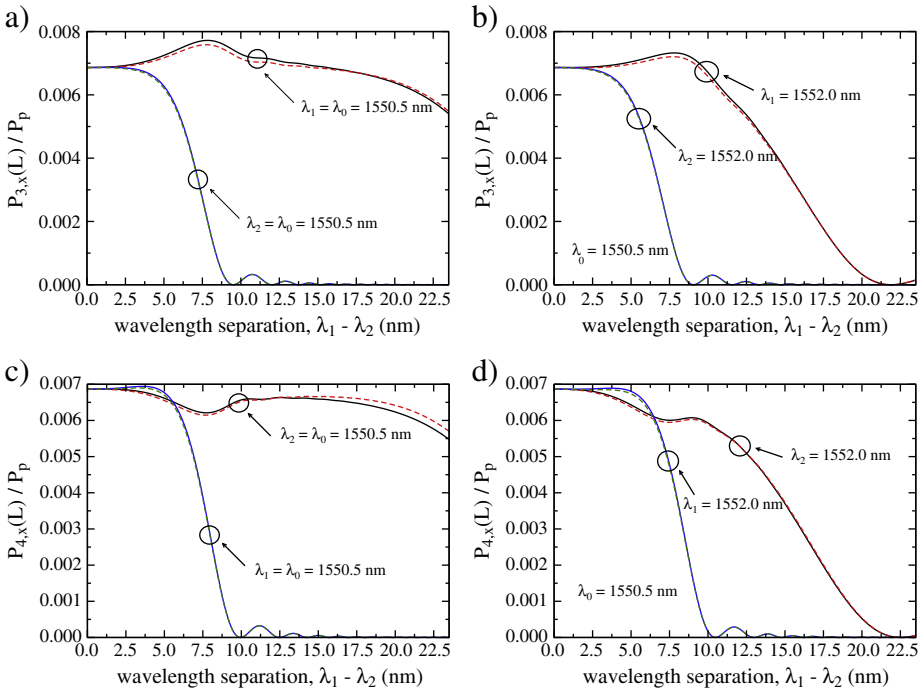

Fig. 2. Optical power evolution for both idler waves, $P_{3,x}(L)$ and $P_{4,x}(L)$ given by Eq. (15) with the wavelength separation $\lambda_1-\lambda_2$. The dashed lines represent the case $f_R=0$, whereas the solid lines represent $f_R=0.245$. Plots a and b describe the idler wave at ω_3, whereas plots c and d show the optical power of the field at ω_4.

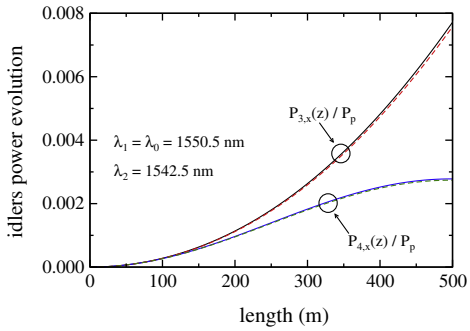

Fig. 3. Optical power evolution for both idler waves along the fiber length. The dashed lines represent the case $f_R=0$, whereas solid lines represent $f_R=0.245$.

Ref. [24]. This is because the dominant process for the generation of the idler wave ω_3 is given by the FWM phase-matching condition $\Delta\beta_{x1}\approx 0$. From Fig. 3, we can also see that the optical power of idler wave at ω_4, $P_{4,x}(z)$, does not grow monotonically along the fiber length. This is due to the fact that the FWM process, given by the FWM phase-matching condition $\Delta\beta_{x2}$ remains unmatched. An analogous result can be achieved if we analyze the generation of the idler waves for $\lambda_2=\lambda_0$ and $\lambda_1=1558.5$ nm.

In Fig. 4, we represent a comparison between this set of multiple FWM processes, given by Eq. (15), and the single and dual pump FWM configurations. The evolution of the idler wave in the single pump FWM configuration is given by [22]

$$P_{3,x}(z)=\left|\gamma\rho_{\parallel}\left(\Omega_{3,1}\right)P_{1,x}z\right|^2P_{2,x}\left|\frac{\sinh\left(r\left(\Omega_{3,1}\right)z\right)}{r\left(\Omega_{3,1}\right)z}\right|^2, \tag{20}$$

where $r^2(\Omega_{3,1})=(\gamma\rho_{\parallel}(\Omega_{3,1})P_{1,x})^2-(K(\Omega_{3,1})/2)^2$, and $K(\Omega_{3,1})=\Delta\beta_{x1}+2\gamma P_{1,x}\rho_{\parallel}(\Omega_{3,1})$. In the case of the dual pump FWM configuration the evolution of the idler wave is given by [22]

$$P_{3,x}(z)=\left|\gamma\eta_{\parallel}(\omega_3)z\right|^2P_{1,x}P_{2,x}P_{4,x}\left|\frac{\sinh\left(g_x(\omega_3)z\right)}{g_x(\omega_3)z}\right|^2. \tag{21}$$

In Fig. 4(a) we represent the evolution of the idler wave at ω_3 with $\lambda_1-\lambda_2$, and in Fig. 4(b) we present the evolution along the fiber length. In Fig. 4(a) and (b), in the single pump configuration ω_3 is the idler, ω_1 is the pump, and ω_2 is the signal wave. In the dual pump configuration ω_3 is the idler, ω_1 and ω_2 are the two pumps and $\omega_4=2\omega_2-\omega_1$ is the signal wave. In both configurations, single and dual pumps, the input signal power is 1 mW, and the input power per pump is 15 mW. In Fig. 4(a), we have used $\lambda_1=\lambda_0$. In Fig. 4(b), we have used $\lambda_1=\lambda_0$ and $\lambda_2=1548$ nm. In both figures the phase-matching condition for the single pump FWM configuration is almost null. In Fig. 4(a) and (b) the multiple FWM processes are given by Eq. (15), and as aforementioned we assume that only the two pumps are launched into the fiber. Results present in Fig. 4 show that the idler wave grows more rapidly in this set of multiple FWM processes than in the single or dual pump FWM configurations. In the single and dual pump configurations the optical power grows of the idler wave is proportional to the square of the pump powers, while in the multiple FWM processes the growth of the idler wave ω_3 involves the cube of the pump powers. This is due to the contribution given by the non-degenerated FWM process for the generation of the idler wave ω_3 in the multiple FWM configurations. Initially (for $z\approx 0$), the generation of the idler wave ω_3 in the multiple FWM configurations arises from the degenerated FWM process given by $2\omega_1=\omega_2+\omega_3$, subsequently the presence of this idler wave will stimulate a non-degenerate FWM process given by $\omega_1+\omega_2=\omega_3+\omega_4$. This can be seen in Eqs. (20) and (21). When $z\approx 0$ $P_{3,x}$ in Eq. (21) is null due to the fact that initially $P_{4,x}$

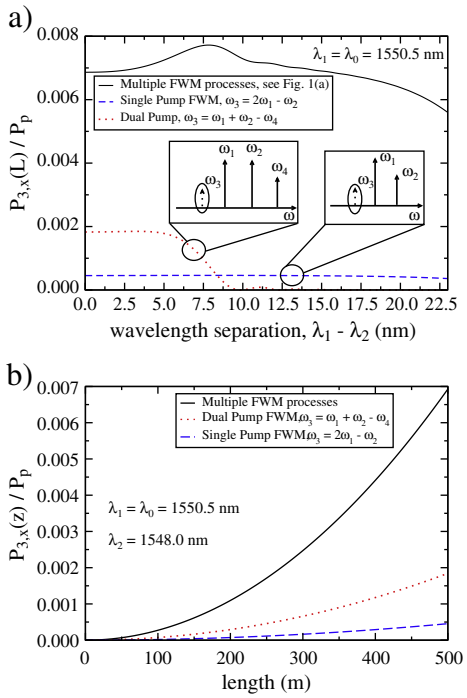

Fig. 4. Comparison between this set of multiple FWM processes, given by Eq. (15), and the typically single and dual pump FWM, with $f_R=0.245$. Plot (a) represents the evolution of the idler wave at ω_3 with $\lambda_1-\lambda_2$, whereas plot (b) shows the evolution along the length of the fiber.

is null. However, $P_{3,x}$ in Eq. (20) is different from zero and the idler wave $P_{3,x}$ starts to grow from the degenerated FWM process $\omega_3=2\omega_1-\omega_2$. At the same time the idler wave $P_{4,x}$ also starts to be generated inside the fiber due to the other degenerated FWM process, given by $\omega_4=2\omega_2-\omega_1$. This can also be seen in Eq. (20), changing the subscript 3 by 4 and exchanging 1 by 2. When the idler waves are generated these degenerated FWM processes give rise to the non-degenerated FWM process described by Eq. (21), which is more efficient than the degenerated FWM process [45]. The combination of all these FWM processes, degenerated and non-degenerated, gives rise to the multiple FWM process, in which the generation of the idler waves is proportional to the cube of the pump power, instead of the square as is the case in Eqs. (20) and (21).

3.2. Idlers evolution in the orthogonal polarization scheme

In the orthogonal polarization scheme and following Eqs. (1) and (4) we find that the evolution of the idler waves in the fiber satisfy the NLS equation

$$\begin{aligned}\frac{\partial A'_{\alpha,j}(z)}{\partial z}&=i\left[k_j(\omega_\alpha)+\gamma\xi_m\left(\Omega_{\alpha,1}\right)P_{1,x}\right]A'_{\alpha,j}(z)\\&+i\gamma\xi_n\left(\Omega_{\alpha,2}\right)P_{2,y}A'_{\alpha,j}(z)+i\gamma\rho_{\perp}\left(\Omega_{\alpha,u}\right)A^2_{u,l}(z)A^*_{v,j}(z)\\&+i\gamma\eta_{\perp}(\omega_\alpha)A_{1,x}(z)A_{2,y}(z)A'^*_{\sigma,l}(z),\end{aligned} \tag{22}$$

where $j\neq l=x,y$, $\alpha\neq\sigma=3,4$ represent the two idlers, according with the notation used in Fig. 1, $u\neq v=1,2$, with $u=1$ for $\alpha=3$ and $u=2$ for $\alpha=4$. For $j=x$ we have $\xi_m=\xi_{\parallel}$ and $\xi_n=\xi_{\perp}$, whereas for $j=y$ we have $\xi_m=\xi_{\perp}$ and $\xi_n=\xi_{\parallel}$. In Eq. (22)

$$\rho_{\perp}\left(\Omega_{\alpha,u}\right)=\frac{1-f_R}{3}+\frac{f_R}{2}\tilde{R}_b\left(\Omega_{\alpha,u}\right), \tag{23}$$

$$\eta_{\perp}(\omega_{\alpha}) = 2\frac{1-f_R}{3} + f_R\tilde{R}_a\left(\Omega_{\alpha,v}\right) + \frac{f_R}{2}\tilde{R}_b\left(\Omega_{\alpha,u}\right). \tag{24}$$

After some mathematical manipulation the evolution of both idlers inside the fiber in this polarization scheme is given by

$$\begin{aligned} P_{\alpha,j}(z) = |A'_{\alpha,j}(z)|^2 = \Bigg|\Bigg\{ e^{i\mathbb{k}_j(\omega_{\alpha})z}\Bigg[i\frac{\gamma\rho_{\perp}\left(\Omega_{\alpha,u}\right)}{g_y(\omega_{\alpha})}A^2_{u,l}A^*_{v,j} \\ \times \sinh\left(g_y(\omega_{\alpha})z\right) + \Theta_{\alpha,y}\left(i\frac{\mathbb{k}_y(\omega_{\alpha})}{g_y(\omega_{\alpha})}\sinh\left(g_y(\omega_{\alpha})z\right) \right. \\ \left. -\cosh\left(g_y(\omega_{\alpha})z\right)\right)\Bigg] + \Theta_{\alpha,y}\Bigg\}\Phi_{\alpha,j}(z)\Bigg|^2, \end{aligned} \tag{25}$$

where

$$\Phi_{\alpha,j}(z) = exp\left\{ i\left[2k_l(\omega_u) - k_j(\omega_v) + \gamma P_{u,l}(2-\xi_{\perp}(0)) - \gamma P_{v,j}(1-2\xi_{\perp}(0)) \right] z \right\}, \tag{26a}$$

$$\begin{aligned} \mathbb{k}_y(\omega_3) = \Big[\Delta\beta_{y1} - \Delta\beta_{y2} + \gamma\left(P_{1,x} - P_{2,y}\right) \\ \times \left(\xi_{\perp}\left(\Omega_{3,1}\right) - \xi_{\parallel}\left(\Omega_{3,2}\right) + 3\xi_{\perp}(0) - 3\right)\Big] / 2, \end{aligned} \tag{26b}$$

$$\begin{aligned} \mathbb{k}_y(\omega_4) = \Big[\Delta\beta_{y2} - \Delta\beta_{y1} + \gamma\left(P_{2,y} - P_{1,x}\right) \\ \times \left(\xi_{\perp}\left(\Omega_{4,2}\right) - \xi_{\parallel}\left(\Omega_{4,1}\right) + 3\xi_{\perp}(0) - 3\right)\Big] / 2, \end{aligned} \tag{26c}$$

$$\begin{aligned} g^2_y(\omega_{\alpha}) = (\gamma\eta_{\perp}(\omega_{\alpha}))^2 P_{1,x}P_{2,y} - \frac{1}{4}\Big[\Delta\beta_{y3} \\ + \gamma\left(P_{1,x} + P_{2,y}\right)\left(\xi_{\parallel}\left(\Omega_{\alpha,v}\right) + \xi_{\perp}\left(\Omega_{\alpha,u}\right) - \xi_{\perp}(0) - 1\right)\Big]^2, \end{aligned} \tag{26d}$$

and

$$\begin{aligned} \Theta_{3,y} = \frac{\gamma^2\eta_{\perp}(\omega_3)\rho_{\perp}\left(\Omega_{3,1}\right)P_{2,y}A^2_{1,x}A^*_{2,y}}{\delta_{\perp}(\omega_3)\varphi_{\perp}(\omega_3) - (\gamma\eta_{\perp}(\omega_3))^2 P_{1,x}P_{2,y}} \\ - \frac{\gamma\varphi_{\perp}(\omega_3)\rho_{\perp}\left(\Omega_{3,1}\right)A^2_{1,x}A^*_{2,y}}{\delta_{\perp}(\omega_3)\varphi_{\perp}(\omega_3) - (\gamma\eta_{\perp}(\omega_3))^2 P_{1,x}P_{2,y}}, \end{aligned} \tag{27a}$$

$$\begin{aligned} \Theta_{4,y} = \frac{\gamma^2\eta_{\perp}(\omega_4)\rho_{\perp}\left(\Omega_{4,2}\right)P_{1,x}A^2_{2,y}A^*_{1,x}}{\delta_{\perp}(\omega_4)\varphi_{\perp}(\omega_4) - (\gamma\eta_{\perp}(\omega_4))^2 P_{1,x}P_{2,y}} \\ - \frac{\gamma\delta_{\perp}(\omega_4)\rho_{\perp}\left(\Omega_{4,2}\right)A^2_{2,y}A^*_{1,x}}{\delta_{\perp}(\omega_4)\varphi_{\perp}(\omega_4) - (\gamma\eta_{\perp}(\omega_4))^2 P_{1,x}P_{2,y}}, \end{aligned} \tag{27b}$$

where

$$\begin{aligned} \delta_{\perp}(\omega_{\alpha}) = \Delta\beta_{y1} + \gamma\left(\xi_{\perp}\left(\Omega_{\alpha,u}\right) + \xi_{\perp}(0) - 2\right)P_{1,x} \\ + \gamma P_{2,y}\left(\xi_{\parallel}\left(\Omega_{\alpha,v}\right) + 1 - 2\xi_{\perp}(0)\right), \end{aligned} \tag{28a}$$

$$\begin{aligned} \varphi_{\perp}(\omega_{\alpha}) = \Delta\beta_{y2} + \gamma\left(\xi_{\perp}\left(\Omega_{\alpha,u}\right) + \xi_{\perp}(0) - 2\right)P_{2,y} \\ + \gamma P_{1,x}\left(\xi_{\parallel}\left(\Omega_{\alpha,v}\right) + 1 - 2\xi_{\perp}(0)\right), \end{aligned} \tag{28b}$$

with

$$\Delta\beta_{y1} = k_y(\omega_3) + k_y(\omega_2) - 2k_x(\omega_1) = 2\frac{\omega_1}{c}\delta n + \Delta\beta_{x1}, \tag{29a}$$

$$\Delta\beta_{y2} = k_x(\omega_4) + k_x(\omega_1) - 2k_y(\omega_2) = -2\frac{\omega_2}{c}\delta n + \Delta\beta_{x2}, \tag{29b}$$

$$\Delta\beta_{y3} = \Delta\beta_{y1} + \Delta\beta_{y2}, \tag{29c}$$

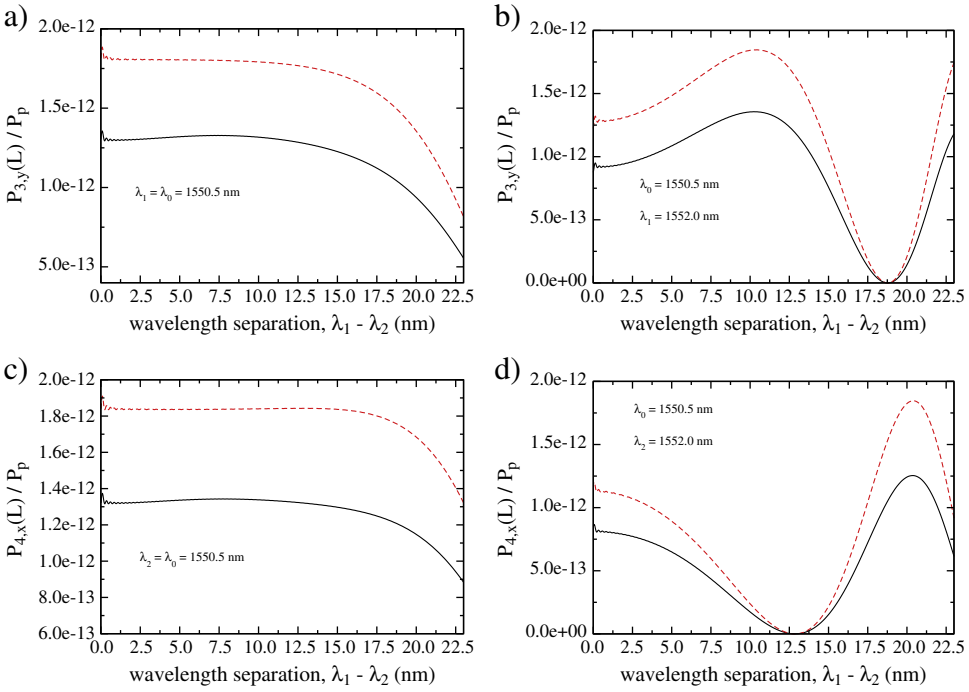

Fig. 5. Optical power evolution for both idler waves in the orthogonal polarization scheme, $P_{3,y}(L)$ and $P_{4,x}(L)$ given by Eq. (25), with $\lambda_1 - \lambda_2$. The dashed line represents the case $f_R = 0$, whereas the solid line represents $f_R = 0.245$. Plots a and b describe the idler wave at ω_3, whereas plots c and d show the optical power of the field at ω_4.

where c is the speed of light in vacuum, and $\Delta\beta_{x1}$ and $\Delta\beta_{x2}$ are given by Eqs. (19a), (19b) and (19c). It was assumed that $A_{\alpha,j}(z=0)=0$, i.e. there are no idler fields at the fiber input.

In Fig. 5 we plot the optical power evolution of both idler waves given by Eq. (25) as a function of wavelength separation between the two pump fields, $\lambda_1-\lambda_2$, in the orthogonal polarization scheme, see Fig. 1(b). In Fig. 5 we can see that the SRS process decreases the optical power of the both idler waves, when compared with the limit $f_R=0$. This arises from the contribution of the imaginary part of $\tilde{R}_a(\Omega_{\alpha,v})$ and $\tilde{R}_b(\Omega_{\alpha,v})$ in the $\Theta_{\alpha,y}$ function, present in Eq. (25).

In Fig. 5(a) and (b), we plot the optical power $P_{3,y}(L)$, given by Eq. (25), as a function of $\lambda_1-\lambda_2$. In Fig. 5(a) we have used $\lambda_1=\lambda_0$, whereas in Fig. 5(b) we have used $\lambda_1=1552$ nm. Results show that the optical power of the idler wave plotted in Fig. 5(a) is higher than the presented in Fig. 5(b). This is due to the fact that the values of $\Delta\beta_{y1}$ and $\Delta\beta_{y2}$ are smaller for $\lambda_1=\lambda_0$, Fig. 5(a), than for $\lambda_1=1552$ nm, Fig. 5(b).

In Fig. 5(c) and in Fig. 5(d), we present the optical power evolution of the idler wave ω_4, given by Eq. (25), as a function of $\lambda_1-\lambda_2$. In Fig. 5 (c) we have used $\lambda_2=\lambda_0$, whereas in Fig. 5(d) we have used $\lambda_2=1552$ nm. Results show that the generation of the idler wave ω_4 is less efficient when neither of the pumps coincide with the fiber zero-dispersion wavelength, Fig. 5(d). This fact emerges from the phase-matching conditions presented in Eqs. (29a), (29b) and (29c) that are closer to zero when $\lambda_2=\lambda_0$.

It can also be seen in Fig. 5 that, this polarization scheme, Fig. 1(b), leads to an inefficient generation of the idler waves at frequencies ω_3 and ω_4, when compared with the co-polarized scheme, Fig. 1(a). This is due to the high value of δn. Decreasing the value of δn, the optical power of the idler waves rapidly increases.

In Fig. 6, we plot the optical power evolution of the idler waves, given by Eq. (25), along 250 m of fiber, in the orthogonal polarization scheme. Fig. 6(a) shows the optical power for the idler wave ω_3, whereas in Fig. 6(b) we present the evolution of $P_{4,x}(z)$. In both figures we have used $\lambda_1=\lambda_0$ and $\lambda_2=1542.5$ nm. Results show that the optical power evolution of both idler waves, $P_{3,y}(z)$ and $P_{4,x}(z)$ is periodic with length. This behavior of the first-order sideband evolution, ω_3 and ω_4, is related with the periodical energy exchange with the pumps. From Fig. 6(a) and (b) we can see that the SRS decreases the efficiency of generation of both idler waves, when compared with the limit $f_R=0$.

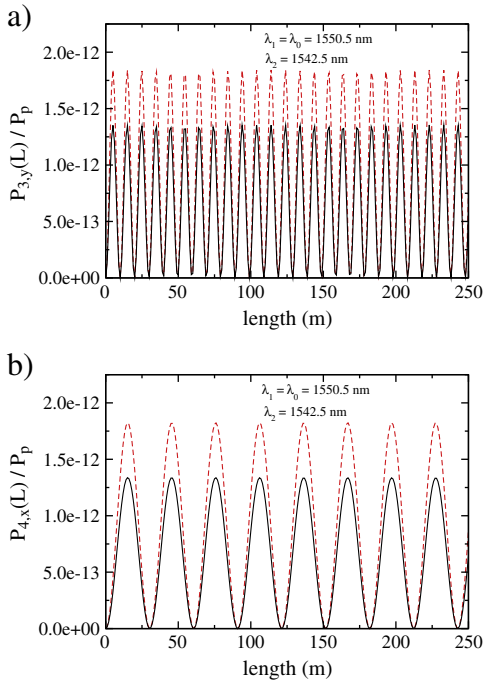

Fig. 6. Optical power evolution for both idler waves along the fiber length. The dashed line represents the case $f_R=0$, whereas the solid line represents $f_R=0.245$. Plot a shows the idler field at ω_3, whereas plot b represents the optical field at frequency ω_4.

4. Polarization sensitivity of the idler waves

In this section we analyze the generation of the idler waves as a function of the polarization angle between the two pumps. The pump at ω_1 is aligned with the x-axis of the fiber. The pump at ω_2 makes an angle ϕ with the x-axis of the fiber [46]. The change of the angle ϕ from 0° to 90° means that we are evolving from the co-polarized to the orthogonal polarization scheme, see Fig. 1. In this scheme the optical power of both idlers at a given z inside the fiber can be written as [46,47]

$$P_3(z) = |A_{3,x}(z)|^2 + |A'_{3,y}(z)|^2, \tag{30}$$

where $|A_{3,x}(z)|^2$ is given by Eq. (15) with $P_{2,x}=P_2cos^2(\phi)$, and $|A'_{3,y}(z)|^2$ is given by Eq. (25) with $P_{2,y}=P_2sin^2(\phi)$, and

$$P_4(z) = |A_{4,x}(z)|^2 + |A'_{4,x}(z)|^2, \tag{31}$$

where $|A_{4,x}(z)|^2$ is given by Eq. (15) with $P_{2,x}=P_2cos^2(\phi)$, and $|A'_{4,x}(z)|^2$ is obtained from Eq. (25) with $P_{2,y}=P_2sin^2(\phi)$.To describe the polarization sensitivity of the generation of the idler waves, we present in Fig. 7 the variation of the optical power of both idler waves with the angle ϕ. Fig. 7 shows the optical power of both idler waves given by Eq. (30) and Eq. (31), for the case $\lambda_1=\lambda_0$ and $\lambda_2=1542.5$ nm. From Fig. 7 we can see that the optical power of $P_3(L)$ and $P_4(L)$ decreases rapidly with the evolution of the angle ϕ. This decreases is more evident for $P_4(L)$ due to the fact that the higher contribution for the generation of the idler wave at ω_4 arises from the photons that are annihilated from the pump P_2. From Fig. 7 we can see that exist a large angle range around $\phi=90^\circ$ where $P_4(L)$ is almost null. This arises from the small contribution given by the orthogonal polarization scheme to the optical power of the idler wave at ω_4. It can also be seenin Fig. 7 that the SRS process does not change significantly the evolution of the idler waves with the angle ϕ.

5. Conclusion

In summary, we investigate the generation of two idler waves inside a HiBi optical fiber, considering three FWM processes and the SRS. Using the coupled-equations we solve analytically the equations that govern the evolution of the complex amplitudes for two pumps inside the fiber, considering that the pumps interact between them through the FWM and SRS processes. We also derive and solve the equations that govern the generation of two idler waves inside an optical birefringent fiber in two polarization schemes. We show that

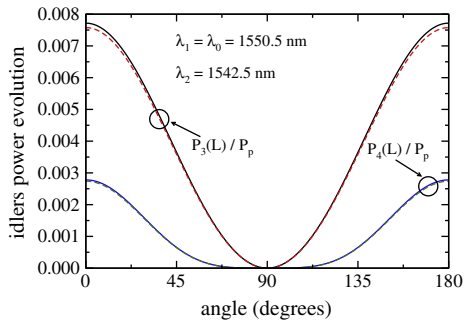

Fig. 7. Optical power of both idler fields, given by Eqs. (30) and (31) respectively, as a function of the polarization angle of the pump wave, ω_2. The dashed lines represent the case $f_R=0$, whereas the solid lines represent $f_R=0.245$.

in the co-polarized scheme the SRS does not change dramatically the optical power evolution of the two idler waves with the wavelength separation between the pumps, even when the pump wavelength coincides with λ_0. We verify that, although one phase-matching condition is almost achieved, two other remain non-phase-matched. We show that the contribution of several FWM processes to the generation of idler wave can increase the efficiency of the process, for certain wavelength detunings. We also show theoretically that the optical power of the idler waves grows monotonically along the fiber length, when the pumps coincide with λ_0. This fact is due to the three FWM contributions to the optical power of the idler wave. The orthogonal polarization scheme leads to an inefficient generation of the idler waves, due to the high value of δn. We verify that the SRS decreases the optical power of the idler waves when compared with limit $f_R = 0$. We show that the evolution from the co-polarized to the orthogonal polarization scheme leads to a continuous loss of efficiency on the generation of the idlers waves.

Results also show that the generation of first-order sidebands from three FWM processes is physically quite different from the typically single and dual pump FWM configurations.

Acknowledgments

This work was supported in part by the Fundação para a Ciência e Tecnologia, FCT, under the PhD Grant SFRH/BD/63958/2009, and by the Instituto de Telecomunicações under the Laboratório Associado program supported by the FCT, and European Union FEDER program, through the IT/LA projects "QuantTel" and PTDC/EEA-TEL/103402/2008 "QuantPrivTel".

References

[1] G.P. Agrawal, Nonlinear Fiber Optics, 3 rd EditionAcademic Press, San Diego, 2001.
[2] A. Martínez-Rios, A.N. Starodumov, Y.O. Barmenkov, V.N. Filippov, I. Torres-Gomez, J. Opt. Soc. Am. B 18 (6) (2001) 794.
[3] M.C. Fugihara, A.N. Pinto, Microwave Opt. Technol. Lett. 50 (2) (2008) 297.
[4] N. Bloembergen, Y.R. Shen, Phys. Rev. Lett. 12 (18) (1964) 504.
[5] R.H. Stolen, J.E. Bjorkholm, A. Ashkin, Appl. Phys. Lett. 24 (7) (1974) 308.
[6] K. Washio, K. Inoue, S. Kishida, Electron. Lett 16 (17) (1980) 658.
[7] C. Lin, W.A. Reed, A.D. Pearson, H.-T. Shang, Opt. Lett. 6 (10) (1981) 493.
[8] X. Sang, P.L. Chu, C. Yu, Opt. Quant. Electron. 37 (10) (2005) 965.
[9] J. Hansryd, P. Andrekson, Photonics Technol. Lett. IEEE 13 (3) (2001) 194.
[10] J.H. Lee, W. Belardi, K. Furusawa, P. Petropoulos, Z. Yusoff, T. Monro, D. Richardson, Photonics Technol. Lett. IEEE 15 (3) (2003) 440.
[11] P. Petropoulos, T.M. Monro, W. Belardi, K. Furusawa, J.H. Lee, D.J. Richardson, Opt. Lett. 26 (16) (2001) 1233.
[12] S. Coen, A.H.L. Chau, R. Leonhardt, J.D. Harvey, J.C. Knight, W.J. Wadsworth, P.S.J. Russell, J. Opt. Soc. Am. B 19 (4) (2002) 753.
[13] A. Siahlo, L. Oxenlwe, K. Berg, A. Clausen, P. Andersen, C. Peucheret, A. Tersigni, P. Jeppesen, K. Hansen, J. Folkenberg, Photonics Technol. Lett. IEEE 15 (8) (2003) 1147.
[14] K. Hansen, J. Jensen, C. Jacobsen, H. Simonsen, J. Broeng, P. Skovgaard, A. Petersson, Optical Fiber Communication Conference and Exhibit, 2002. OFC 2002, 2002, p. FA9-1.
[15] F. Poli, A. Cucinotta, S. Selleri, Photonic Crystal Fibers: Properties and Applications, 1st EditionSpringer, Netherlands, 2007.
[16] K.O. Hill, D.C. Johnson, B.S. Kawasaki, R.I. MacDonald, J. Appl. Phys. 49 (10) (1978) 5098.
[17] N. Shibata, R. Braun, R. Waarts, Quant. Electron. IEEE J. 23 (7) (1987) 1205.
[18] N.A. Silva, N.J. Muga, A.N. Pinto, Quant. Electron. IEEE J. 46 (3) (2010) 285.
[19] K. Blow, D. Wood, Quant. Electron. IEEE J. 25 (12) (1989) 2665.
[20] S. Trillo, S. Wabnitz, J. Opt. Soc. Am. B 9 (7) (1992) 1061.
[21] R. Stolen, J. Bjorkholm, Quant. Electron. IEEE J. 18 (7) (1982) 1062.
[22] N. Silva, N. Muga, A. Pinto, Lightwave Technol. J. 27 (22) (2009) 4979.
[23] J.R. Thompson, R. Roy, Opt. Lett. 16 (8) (1991) 557.
[24] J.R. Thompson, R. Roy, Phys. Rev. A 43 (9) (1991) 4987.
[25] J.R. Thompson, R. Roy, Phys. Rev. A 44 (11) (1991) 7605.
[26] D.L. Hart, A. Judy, T.A.B. Kennedy, R. Roy, K. Stoev, Phys. Rev. A 50 (2) (1994) 1807.
[27] S. Trillo, S. Wabnitz, T.A.B. Kennedy, Phys. Rev. A 50 (2) (1994) 1732.
[28] D.L. Hart, A.F. Judy, R. Roy, J.W. Beletic, Phys. Rev. E 57 (4) (1998) 4757.
[29] G. Millot, Opt. Lett. 26 (18) (2001) 1391.
[30] B. Khubchandani, P.N. Guzdar, R. Roy, Phys. Rev. E 66 (6) (2002) 066609.
[31] X. Liu, X. Zhou, C. Lu, Phys. Rev. A 72 (1) (2005) 013811.
[32] X.-M. Liu, Phys. Rev. A 77 (4) (2008) 043818.
[33] J. Hansryd, P. Andrekson, M. Westlund, J. Li, P.-O. Hedekvist, IEEE J. 8 (3) (2002) 506.
[34] K. Inoue, H. Toba, Photonics Technol. Lett. IEEE 4 (1) (1992) 69.
[35] A. Hasegawa, Opt. Lett. 9 (7) (1984) 288.
[36] P. Andrekson, N. Olsson, J. Simpson, T. Tanbun-Ek, R. Logan, M. Haner, Electron. Lett 27 (11) (1991) 922.
[37] P. Hedekvist, P. Andrekson, Electron. Lett 32 (9) (1996) 830.
[38] A. Yariv, D. Fekete, D.M. Pepper, Opt. Lett. 4 (2) (1979) 52.
[39] P. Hedekvist, M. Karlsson, P. Andrekson, Photonics Technol. Lett. IEEE 8 (6) (1996) 776.
[40] P.V. Mamyshev, S.V. Chernikov, Opt. Lett. 15 (19) (1990) 1076.
[41] R.W. Hellwarth, Prog. Quant. Electron. 5 (1977) 1.
[42] Q. Lin, G.P. Agrawal, Opt. Lett. 31 (21) (2006) 3086.
[43] R.H. Stolen, M.A. Bösch, C. Lin, Opt. Lett. 6 (5) (1981) 213.
[44] Q. Lin, F. Yaman, G.P. Agrawal, Phys. Rev. A At. Mol. Opt. Phys. 75 (2) (2007) 023803.
[45] B.P. Pal, Ch. Fiber-Optic Parametric Amplifiers for Lightwave Sysytems, Academic Press, San Diego, 2005, p. 101.
[46] C.J. McKinstrie, S. Radic, C. Xie, J. Opt. Soc. Am. B 20 (7) (2003) 1437.
[47] N.J. Muga, N.A. Silva, M.F. Ferreira, A.N. Pinto, Opt. Commun. 283 (10) (2010) 2125.